

Introduction to Molecular-Scale Understanding of Surface Tension

Yasutaka Yamaguchi, Hiroshi Kawamura

Abstract In this article, microscopic understanding of the surface tension are provided, which needs basic knowledge of thermodynamics, statistical mechanics as well as continuum mechanics. By introducing the intermolecular interaction potential and temperature definition, and by showing conceptual pictures including some results obtained by molecular dynamics simulations, the author hopes that the target readers of undergraduate level students can find fascinating aspects of surface tension as the boundary of macroscopic and microscopic physics.

1 Introduction

Liquids are supposed to be incompressible due to their small compressibility, *e.g.*, its value of water is about $5 \times 10^{-10} \text{ Pa}^{-1}$. Thus, when liquids are in an open space or in a closed space with a volume larger than theirs, they dispose solid-liquid

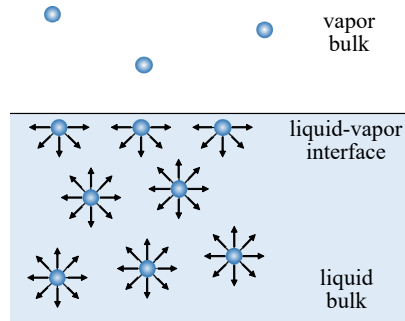


Fig. 1 Schematic for the molecular scale explanation of the surface tension.

Yasutaka Yamaguchi
Department of Mechanical Engineering, 2-1 Yamadaoka, Suita 565-0871, Japan e-mail:
yamaguchi@mech.eng.osaka-u.ac.jp

and/or solid-gas interfaces, hence, liquids we see in our daily life almost always have interface. Interfacial tensions are termed as the force exerted on such interfaces.

At present, the existence of molecules is commonly accepted, and the mechanism of the liquid-vapor (LV) or liquid-gas (LG) surface tension, known as a tensile force at the interface, is usually explained by using a schematic as exemplified in Fig. 1. As in this figure, the molecules around the liquid-vapor interface have less partners to interact with than those in liquid bulk, and the liquid-vapor interface is generally disadvantageous to liquid bulk. This seems to be simple and intuitively understandable; however, as Ref. [1] pointed out, Fig. 1 with the arrow directing outward the molecules gives an impression that molecules in the liquid bulk and at the liquid-vapor interface ‘pull’ each other, and the molecule at the interface is subject to a net force along the direction perpendicular to the interface, not a force parallel to the interface. This kind of confusing questions are often posed especially for interfacial phenomena, and indeed, I personally think this is one of the fascinating aspects of interface physics which includes macroscopic and microscopic features.

In this article, basic pictures for understanding of the surface tension are provided with some simulation results, This concept is similar to Refs. [1] and [2], basically targeting undergraduate level students, contrary to many other textbooks on this subject; however, I believe that basic but wide and throughout outlook of thermodynamics, statistical mechanics and continuum mechanics is needed to understand the physics of interface, and more importantly, to avoid misleading which also have trapped professional scientists [3]. Partly related to this point, molecular dynamics (MD) simulations have become common especially with the development of high-performance computers and simulation packages including LAMMPS [4] and GROMACS [5] from the beginning of the 21st century, and we can easily have access to the movies of various (colorful) molecules. The great scientists in the history could not have such movies, and they had to imagine basically from macroscopic experimental results; however, this does not mean that we will not be trapped by the misunderstanding. To advance science, we have to make use of both the robust theories constructed by the great scientists in the history and computer simulations to extend our understanding.

2 Brief history

Although there are several opinions about the origin of the study of capillarity or surface tension [2, 6, 7], scientific and mathematical approach toward its understanding through the modeling of wetting started from the beginning of the 19th century with T. Young (1773–1829) and P.-S. Laplace (1749–1827). In 1805, Young proposed the following equation [8]

$$\gamma_{SL} - \gamma_{SV} + \gamma_{LV} \cos \theta = 0, \quad (1)$$

where γ_{SL} , γ_{SV} and γ_{LV} are the solid-liquid, solid-vapor, and liquid-vapor interfacial tensions, respectively, and θ is the contact angle as the angle between the SL and LV

interfaces. Equation (1) is called Young’s equation. Although his original article [8], indeed in “essay” style, has only one table and gives no equation nor figure, Eq. (1) was originally suggested to express the force balance parallel to the solid surface exerted on the contact line as shown in Fig. 2. Note that the proposal of Young’s equation (1) is sometimes referred to as in 1804, because he made a talk about this topic in this year. Young’s equation (1) was extended to evaluate wettability of a liquid on a solid surface, known as the Young-Dupré equation:

$$S = \gamma_{LV}(\cos \theta - 1), \quad (2)$$

where the spreading coefficient S given by

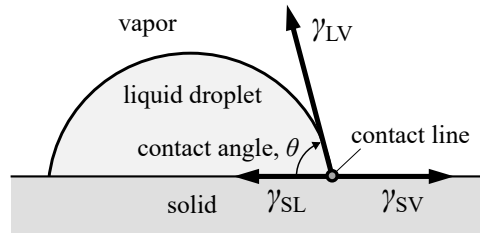
$$S = \gamma_{SV} - (\gamma_{SL} + \gamma_{LV}) \quad (3)$$

expresses the wettability: $S = 0$ gives $\cos \theta = 1$ in Eq. (2) and positive S means that the liquid completely covers the solid surface.

The year of 1804 or 1805 was before the establishment of thermodynamics: N. L. S. Carnot (1796–1832) was under ten, and J. P. Joule (1818–1881), W. Thomson (Lord Kelvin, 1824–1907) R. Clausius (1822–1888), and J. W. Gibbs (1839–1903) were not born, and this clearly means that Young did not and could not bring the concept of thermodynamics nor molecular interaction into his modelling of wetting and surface tension as shown in Fig. 1 [3]. Note that the primary hydrodynamic description summarized in “Hydrodynamica” by D. Bernoulli (1700–1782) [9], which was based on Newtonian mechanics by I. Newton (1642–1727), was already published at that time, and the Euler Equations about ideal fluids by L. Euler (1707–1783) as the mathematical framework of fluid mechanics as well as the Lagrangian mechanics by J.-L. Lagrange (1736–1813) were already available [10]. Probably, continuum mechanics including the concept of stress tensor was not available considering the ages of A.-L. Cauchy (1789–1857), C. L. M. H. Navier (1785–1836) and S. D. Poisson (1781–1840).

Anyway, by the frontiers including the above-mentioned scientists, thermodynamics was established in the 19th century, and based on it, the van der Waals equation of state expressing the phase coexistence was proposed by J. D. van der Waals (1837–1923). He also wrote an article about surface tension in 1893 [11, 12], and introduced the concept of dividing surface and formulated a thermodynamic framework with a liquid-vapor interface. Just after the tragedy of L. Boltzmann (1844–1906), J. Perrin

Fig. 2 Schematic of Young’s equation proposed as the surface lateral force balance of interfacial tensions exerted on the contact line.



(1870–1942) experimentally proved the existence of molecules inspired by the idea of A. Einstein (1879–1955) [10], and this enabled the above-mentioned explanation of the surface tension through the interaction potential between molecules interacting with a potential well depth, *i.e.*, with a moderate attraction force for long intermolecular distance range and a strong repulsion for short distance range described in detail below. Based on this interaction potential model, G. Bakker (1856–1938), R. C. Tolman (1881–1948), J. G. Kirkwood (1907–1959), F. P. Buff (1924–2009), etc. constructed the theoretical framework of the surface tension in thermodynamic equilibrium. Note that Japanese scientists including S. Ono (1918–1995), S. Kondo (1922–2014), A. Harashima (1908–1986), etc. largely contributed to the development. Especially, Ono and Kondo wrote a great review [13], and they categorized the approaches of surface tension into thermodynamic and quasi-thermodynamic ones, statistical mechanical ones and hydrodynamic (also mentioned as “mechanical” in [7]) ones. Ono also left an instructive textbook in Japanese [7], and he wrote in the introduction of the book: “surface is very thin but still has thickness, and it is a pity that its physics is difficult to understand because of this fact.” This sentence clearly points out the difficulty of surface, and also shows the fascinating feature of surface physics. Another great textbook by J. S. Rowlinson and B. Widom [14] is also available; indeed, the history in the present article mentioned above is based on these books [7, 14].

As described above, it is basically necessary to include the microscopic concept to fully explain or understand the mechanism of surface tension and wetting. On the other hand, as we see water droplets on solid surfaces almost everyday, such a liquid motion affected by the surface tension is very common and macroscopic, *i.e.*, visible by bare eyes. As Young modelled, it is possible to understand and predict the macroscopic liquid behavior by simply considering the surface tension as the force to reduce the surface area without the above-mentioned microscopic knowledge. Indeed in the middle of 18th century, an experimental approach to measure the surface tension was proposed by L. F. Wilhelmy (1812–1864). In this method called the Wilhelmy plate method [15], which is commonly used also at present, a solid plate or a cylinder is vertically immersed into a liquid pool, and the surface tension is evaluated by measuring the contact angle and the vertical force exerted on the solid. This standpoint is equivalent to the above-mentioned hydrodynamics approach that Ono and Kondo categorized, in which the microscopic physics of interface with non-zero thickness is integrated into the surface tension on a surface with zero thickness. As the name indicates, this hydrodynamic implementation matches well with the governing equations of fluid dynamics, and is especially familiar with the numerical simulation technique called the computational fluid dynamics (CFD). In practice, thermodynamic and statistical mechanical approaches cannot be applied for dynamic systems in principle because these approaches assume static thermodynamic equilibrium. Anyway, CFD simulations of liquid flow with moving interface are common at present owing to the development of high-speed computers from 1980s.

Parallel to the CFD, the (classical) molecular dynamics (MD) method, which solves the motion of constituent molecules of fluids governed by inter-molecular

potential functions based on the Newtonian mechanics, has also been developed, and this method enabled the simulations of liquid behavior with interfaces as a microscopic approach. Indeed, one can obtain an equilibrium liquid-vapor coexistence system with an interface by locating a certain number of molecules in a simulation cell, whose intermolecular force is given by a potential function exemplified in Fig. 3, and by controlling the temperature of the system. As pointed out in Ref. [14], this solves the main difficulty in the statistical mechanical approach of how to analytically obtain the equilibrium density distribution in such liquid-vapor coexistence system from the microscopic intermolecular potential function.

3 Why phase separation happens and why interface is formed – from thermodynamics –

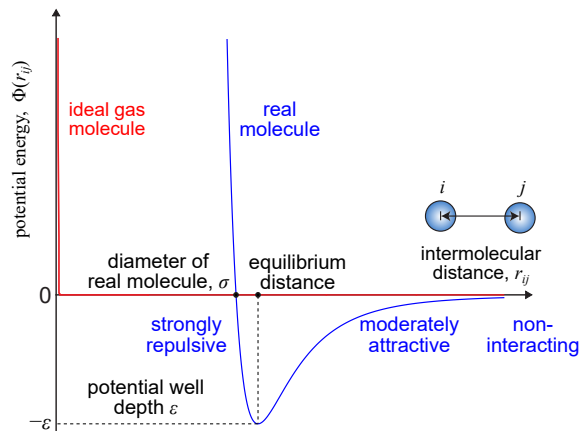
3.1 Ideal gas model and temperature

In order to understand the properties of the liquid-vapor interface, a primitive question of why the constituent molecules try to gather to form liquid and vapor phases having different densities as illustrated in Fig. 1 instead of forming a single homogeneous phase with a uniform density. Indeed, a fluid which always stays single homogeneous phase exists as a conceptual one: an ideal gas. The principal (macroscopic) definition of ideal gases is that they always obeys the equation of state:

$$pV = nRT, \quad (4)$$

where p , V , n , T and R denote the pressure, the volume, the amount of substance of the gas in moles, the absolute temperature, and the universal gas constant, respectively.

Fig. 3 Intermolecular interaction between ideal gas molecules and between real molecules. No intermolecular force acts between ideal gas molecules and they have no volume. On the other hand, real molecules are generally attracted by each other for an intermediate interatomic distance and repelled for a smaller distance around the molecular diameter, and they have almost no interaction for a longer distance. The minimum point of the potential energy is the equilibrium distance.



Indeed, Eq. (4) holds under high temperature and low pressure conditions for real gases, and an ideal gas model is an extended imaginary substance which obeys Eq. (4) irrespective of the temperature and pressure. D. Bernoulli was the first to propose the basis for the kinetic theory of gases in his book of *Hydrodynamica* [9] in the 18th century. In this book, he argued that a gas consists of a huge number of molecules moving in all directions, and their impact on a surface causes the pressure of the gas, and thus their average kinetic energy determines the temperature of the gas under the following assumptions:

- The constituent molecules of the gas are infinitesimally small hard spheres, besides they are subject to elastic collisions among each other and with the surroundings (container wall).
- There are no attractive or repulsive forces between the molecules apart from those that determine their point-like collisions, *i.e.*, the only forces between the gas molecules and the surroundings are impulsive force upon the point-like collisions.
- The molecules are constantly moving, and as a result of multiple random collisions, their velocity distribution reaches a certain isotropic random directions as an equilibrium state.

Almost after a century, the idea was revisited in the 19th century by Clausius and J. C. Maxwell (1831–1879), etc. From the assumption above, it is possible to relate the mean square velocity of the constituent molecules $\langle |\mathbf{v}|^2 \rangle$ with the pressure p with the density ρ of the gas in three-dimension as

$$p = \frac{\rho \langle |\mathbf{v}|^2 \rangle}{3} \quad (5)$$

by considering the sum of impulse exerted from the molecules on the container wall of unit area per unit time, where $\langle |\mathbf{v}|^2 \rangle$ is defined as the space, temporal and molecular average by

$$\langle |\mathbf{v}|^2 \rangle \equiv \lim_{t_\infty \rightarrow \infty} \frac{1}{t_\infty} \int_0^{t_\infty} \left[\frac{1}{N} \sum_{i=1}^N |\mathbf{v}_i|^2 \right] dt \quad (6)$$

for N molecules with the velocity of i -th molecule being \mathbf{v}_i . Note that \mathbf{v}_i satisfies

$$\frac{1}{N} \sum_{i=1}^N \mathbf{v}_i = \mathbf{0} \quad (7)$$

for present equilibrium gases, *e.g.*, confined in a closed container. In case the container is moving at a constant velocity, $\langle |\mathbf{v}|^2 \rangle$ must be defined by using the molecular velocities relative to the group motion. By the way, the relation in Eq. (5) derived by Clausius is amazing because the speed of invisible molecules can be estimated only by the two measurable macroscopic values of the pressure p and the density ρ [10]. By inserting Eq. (5) into Eq. (4), it follows

$$M \langle |\mathbf{v}|^2 \rangle = 3RT, \quad (8)$$

where M denotes the mass of gas per mole. Then, let m and k_B be the mass of single molecule and the Boltzmann constant, respectively defined by

$$m \equiv \frac{M}{N_A}, \quad k_B \equiv \frac{R}{N_A} = 1.38 \times 10^{-23} \text{ J/K} \quad (9)$$

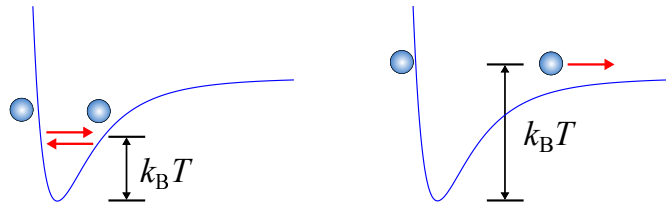
using the Avogadro number N_A , we obtain a fundamental relation between the kinetic energy of the constituent molecule and the absolute temperature:

$$\frac{1}{2}m \langle |\mathbf{v}|^2 \rangle = \frac{3}{2}k_B T. \quad (10)$$

Equation (10) can be extended to real molecules as the microscopic definition of temperature T .

3.2 Intermolecular potential

The intermolecular interaction between ideal gas molecules can be schematically illustrated in Fig. 3 with the red line. The horizontal line for overall distance except at zero distance shown with the vertical line indicates that the molecules have no interaction force except the hard point-like collision. In contrast to this ideal gas feature, the interaction potential between real molecules can be modeled as the blue line in Fig. 3. Two real molecules within an intermediate intermolecular distance attract each other whereas a strong repulsive force acts between the two within a smaller distance around the molecular diameter, and they have almost no interaction for a longer distance. The distance giving the minimum potential energy of $-\varepsilon$ is the equilibrium distance.



Solid or Liquid:
molecules are trapped in the potential well and they stay near at low T .

Gas (critical state for high density):
molecules are apart from each other and have no interaction at high T & low ρ (low p).

Fig. 4 Schematic of the intuitive understanding of the temperature-dependent phase change from intermolecular interaction between real molecules. Left: molecules are trapped in the potential well because the average kinetic energy corresponding to $k_B T$ is not sufficiently large. Right: molecules can escape from the potential well with the kinetic energy and freely moving in a ballistic manner. The left corresponds to the solid or liquid phase whereas the right is the gas phase.

Now we try to intuitively understand phase change from this interaction potential of real molecules with a potential well depth and the definition of absolute temperature T in Eq. (10). Figure 4 shows the schematic for the understanding of the temperature-dependent phase change from the intermolecular interaction between real molecules. Suppose two molecules vibrating around the potential well at a low temperature without total translational motion as in the left panel, *i.e.*, satisfying Eq. (7). Then, as indicated by Eq. (10), the two molecules have certain relative average kinetic energy with a scale of $k_B T$.

At a low temperature with the corresponding kinetic energy sufficiently smaller than the potential well depth ε , the molecules are trapped in the potential well. In that case, molecules rarely change their interaction pairs and if there more than two molecules, they try to maximize the number of neighboring pairs to minimize the potential energy, and they eventually form a solid crystal typically with a closed packing structure. Note that thermal expansion of solid can also be understood from the asymmetric vibration feature around the equilibrium point; the intermolecular distance at $T = 0$ is apparently at the minimum of the potential well while the time-averaged mean distance at $T > 0$ becomes longer as the temperature increases. This expansion is not expected if the intermolecular interaction is modeled by a simple harmonic spring connecting the two molecules, which gives a symmetric vibration around the point of minimum potential energy.

Under a moderate temperature, molecules can frequently escape from the potential well and change the pairs without having certain fixed structures. This can be understood as liquid. At high temperature as shown in the right panel of Fig. 4, molecules are not trapped in the potential well due to their sufficient kinetic energy and freely moving in space. This corresponds to the gas phase.

Hence, the key features of real molecules can be summarized as follows:

- There are short-range repulsive and long range attractive forces between the molecules to form a potential well.
- The molecules are constantly moving, and as a result of multiple random collisions, their velocity distribution reaches a certain isotropic random directions as an equilibrium state.

The second feature is the same as ideal gases and the kinetic energy of the random motion is equally distributed to each degree of freedom: the equipartition under thermal equilibrium as a primitive basis of statistical mechanics. It is easy to imagine why Eq. (4) holds under high temperature and low pressure conditions for real gases from the intermolecular interaction potential of real molecules; however, the history of thermodynamics and statistical mechanics tells that constructing it from ideal gas potential is not that easy. Indeed, the outstanding idea of D. Bernoulli that gases as fluid consist of huge number of infinitesimally small molecules, proposed in the first half 18th century was not further investigated for about a century until Clausius and Maxwell [10].

Anyway, now we go back to the interpretation of the surface tension in Fig. 1. This figure does not mean that the molecular pairs in the liquid bulk pull the partner molecule each other but they are at a certain mean inter-molecular distance as

indicated in the right panel of Fig. 3. Molecules around the interface have less partners to interact with than those in the liquid bulk, and those in the vapor bulk have almost no partners. As mentioned above, with the present computers, MD simulations can be easily run even with a laptop computers. Figure 5 shows the snapshot of equilibrium systems consisting of molecules with their intermolecular interaction described by the Lennard-Jones potential popularly used as a simple model expressing the above-mentioned feature:

$$\Phi_{\text{LJ}}(r_{ij}) = 4\varepsilon \left[\left(\frac{\sigma}{r_{ij}} \right)^{12} - \left(\frac{\sigma}{r_{ij}} \right)^6 \right], \quad (11)$$

where ε and σ denote the potential well depth and diameter shown in Fig. 3. One thousand molecules are confined in a cubic box sized $30\sigma \times 30\sigma \times 30\sigma$ with the time-averaged system temperatures, *i.e.*, kinetic energy given by Eq. (10), set at $k_{\text{B}}T/\varepsilon$ equal to 0.75 and 1.5 in the left and right systems, respectively.

Note that the molecules in the systems are constantly moving as described above, and even if one starts a simulation from arbitrary initial configuration, for instance, with locating the molecules at grid points, the molecules spontaneously form corresponding equilibrium states after a certain time as in the snapshots. This term ‘equilibrium’ in the microscopic scale roughly means that the molecules are moving with the positions and momenta of the constituent molecules changing with time, but their apparent feature as a group is unchanged. For instance, most of the con-

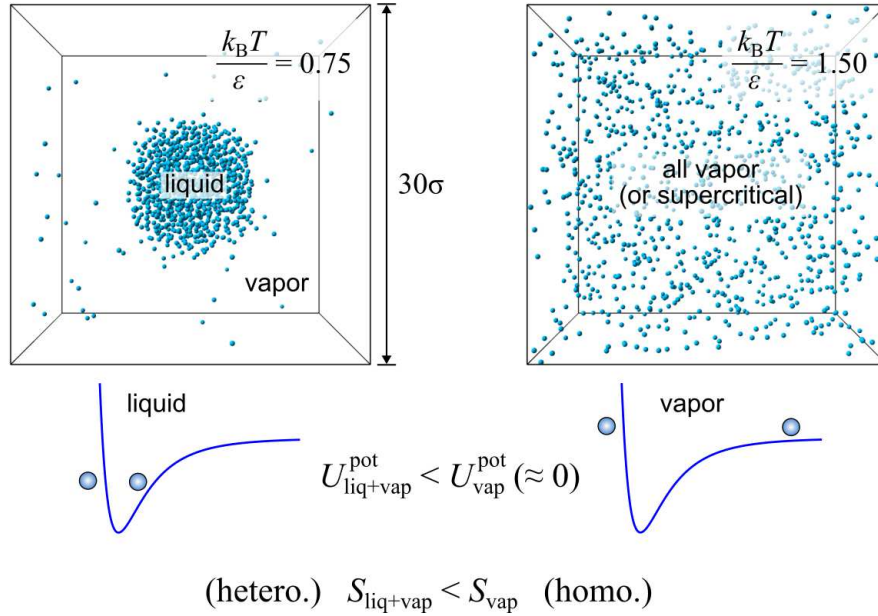


Fig. 5 MD simulation results of simple Lennard-Jones molecules confined in a calculation cell.

stituent molecules are gathered to form a spherical liquid droplet with remaining molecules flying as vapor around the droplet in the left system as an equilibrium state; the constituent molecules of liquid and vapor change but the volume as well as the spherical structure of the droplet are unchanged. Similarly, the positions of momenta of the molecules change, but they always keep vapor phase in the right system after reaching the equilibrium state spontaneously achieved after a certain time irrespective of the initial condition. As described later, this spontaneous change of the system is due to the minimization of the Helmholtz free energy of the system.

As clearly observed from the figure, liquid-vapor coexistence kept at the lower temperature of $k_B T/\varepsilon = 0.75$ in the left panel is lost with the temperature rise, and the system is filled with vapor (indeed supercritical phase) at the higher temperature of $k_B T/\varepsilon = 1.5$. This phase change can be intuitively understood from the schematic in Fig. 4.

We further think about why the droplet in the left panel takes the spherical structure to minimize the surface area from an energetic point of view. Let the potential energy per molecule in the vapor bulk, at the LV interface, and in the liquid bulk be e_V , e_{LV} and e_L , respectively. Then, they satisfy

$$e_L < e_{LV} \ll e_V \approx 0 \quad (12)$$

considering the schematic in Fig. 1 and intermolecular potential in Fig. 3, which indicates that e_V , e_{LV} are basically negative whilst e_L is almost zero for molecules in the vapor phase without partners to interact with. The first inequality implies that the number of neighbouring molecules is smaller at the interface than in the liquid bulk. Consequently

$$e_V - e_{LV} > 0 \quad (13)$$

holds. In addition, let the number of corresponding molecules and volumes being N_L , N_{LV} and N_V , and V_L , V_{LV} and V_V , respectively. Then, the number of molecules N and volume V of the system write

$$N = N_L + N_{LV} + N_V \quad (14)$$

and

$$V = V_L + V_{LV} + V_V, \quad (15)$$

respectively. In the macroscopic scale, we assume $N_{LV} = 0$ and $V_{LV} = 0$ while the LV interface is a region in the molecular scale and molecules indeed exist there. We define the corresponding volumes per molecule as

$$v_L = \frac{V_L}{N_L}, \quad v_{LV} = \frac{V_{LV}}{N_{LV}}, \quad v_V = \frac{V_V}{N_V}. \quad (16)$$

Assuming that v_{LV} is approximately the same as v_L , it follows for the volume per molecule that

$$0 < v_L \approx v_{LV} \ll v_V. \quad (17)$$

Then, Eq. (15) rewrites

$$V = N_V v_V + N_{LV} v_{LV} + N_V v_L \approx (N_L + N_{LV}) v_L + N_V v_V. \quad (18)$$

On the other hand, the internal energy U of a system is separated into the kinetic and potential contributions U^{kin} and U^{pot} , respectively as

$$U = U^{\text{kin}} + U^{\text{pot}}. \quad (19)$$

Using Eq.(10), the former is given by

$$U^{\text{kin}} \equiv \sum_{i=1}^N \frac{1}{2} m |\mathbf{v}_i|^2 = \frac{3}{2} N k_B T, \quad (20)$$

which is constant under the constant temperature condition. The latter of potential term is formally given by

$$U^{\text{pot}} \equiv \sum_{i=1} \sum_{j(>i)} \Phi(r_{ij}). \quad (21)$$

This can be approximated using the mean potential energy per molecule as

$$\begin{aligned} U^{\text{pot}} &\approx N_V e_V + N_{LV} e_{LV} + N_L e_L \\ &= (N_L + N_{LV}) e_L + N_{LV} (e_{LV} - e_L). \end{aligned} \quad (22)$$

From Eqs. (18)-(22) and Inequality (13), it is shown that with keeping $N_L + N_{LV}$ constant, reducing the internal energy U in Eq. (22) is possible by decreasing N_{LV} without changing the volume V in Eq. (18). This means that the system internal energy can be reduced by decreasing the surface area A_{LV} because N_{LV} is apparently proportional to A_{LV} . This leads to the formation of the spherical droplet in the left panel of Fig. 5 as an equilibrium shape with the smallest surface area in the three-dimensional space.

3.3 Free energy and entropy

The explanation above looks reasonable; however, another question arises why the system prefers to take the ‘all vapor’ state with less internal energy U at higher temperatures. The trap model in Fig. (4) merely indicates that the molecular pairs easily dissociate from each other, but they can have a lower internal energy even at a higher temperature if they form more intermolecular pairs. To answer this question, the free energy instead of the internal energy must be considered. The second law of thermodynamics tells us that the Helmholtz free energy F of a system given by

$$F \equiv U - TS \quad (23)$$

decreases until the system reaches the equilibrium state, *i.e.*,

$$dF \leq 0 \text{ (nonequilibrium)}, \quad F = F_{\min} \text{ (equilibrium)} \quad (24)$$

holds for F for a system under constant volume V and constant temperature T condition. This corresponds to a closed container in contact with a constant-temperature heat bath. The key point is that the Helmholtz free energy in Eq. (23) includes the entropy of the system S .

In classical statistical mechanics, the entropy S is related to the “number of possible equivalent microstates corresponding to a certain macroscopic state” Ω as follows:¹

$$S = k_B \ln \Omega, \quad (25)$$

where a microstate in 3-dimensional system of N -molecules is determined by giving $3N$ -positions and $3N$ -momenta of constituent molecules. From Eq. (25), it is possible to show that the position contribution to entropy S is the largest for a system with homogeneous density. We will see that in the following example:

(Example) Suppose a closed equilibrium system with ideal gas molecules in a box at a constant temperature, and let N_{left} and N_{right} be the numbers of gas molecules in the left-half and right-half of a box, respectively, and denote the case by $[N_{\text{left}}, N_{\text{right}}]$ ($N = N_{\text{left}} + N_{\text{right}}$). Evaluate the number of possible cases and compare the two for the following three cases, respectively:

1. Case of small total number $N_{\text{total}} = 200$: $[99, 101]$ vs. $[100, 100]$
2. Case of a larger total number $N_{\text{total}} = 2000$: $[990, 1010]$ vs. $[1000, 1000]$
3. Case of a huge (Avogadro scale) total number of $N_{\text{total}} = 2 \times 10^{23}$: $[0.99N_A, 1.01N_A]$ vs. $[N_A, N_A]$

(Answer) The numbers of cases Ω to separate $N_{\text{left}} + N_{\text{right}}$ into left and right are given by

1. $N_{\text{total}} = 200$:

$$\begin{aligned} \Omega_{[99,101]} &= \frac{200!}{99!101!}, & \Omega_{[100,100]} &= \frac{200!}{100!100!} \\ \frac{\Omega_{[99,101]}}{\Omega_{[100,100]}} &= \frac{100!100!}{99!101!} = \frac{100}{101} \end{aligned}$$

2. $N_{\text{total}} = 2000$:

$$\begin{aligned} \Omega_{[990,1010]} &= \frac{2000!}{990!1010!}, & \Omega_{[1000,1000]} &= \frac{2000!}{1000!1000!} \\ \frac{\Omega_{[990,1010]}}{\Omega_{[1000,1000]}} &= \frac{1000!1000!}{990!1010!} = \frac{991}{1001} \cdot \frac{992}{1002} \cdots \frac{1000}{1010}, \end{aligned}$$

The ratio above satisfies

¹ Boltzmann’s tombstone bears the inscription of ‘ $S = k \log W$ ’.

$$\left(\frac{99}{100}\right)^{10} < \frac{\Omega_{[990,1010]}}{\Omega_{[1000,1000]}} < \left(\frac{100}{101}\right)^{10} \quad \therefore \frac{\Omega_{[990,1010]}}{\Omega_{[1000,1000]}} \approx \left(\frac{99}{100}\right)^{10}$$

3. $N_{\text{total}} = 2 \times 10^{23}$:

$$\begin{aligned} \Omega_{[0.99N_A, 1.01N_A]} &= \frac{2N_A!}{(0.99N_A)!(1.01N_A)!}, & \Omega_{[N_A, N_A]} &= \frac{2N_A!}{N_A!N_A!} \\ \frac{\Omega_{[0.99N_A, 1.01N_A]}}{\Omega_{[N_A, N_A]}} &= \frac{N_A!N_A!}{(0.99N_A)!(1.01N_A)!} \approx \left(\frac{99}{100}\right)^{0.01N_A} \end{aligned} \quad (26)$$

Equation (26) indicates that the probability to see 2 % density difference ($0.99\rho_0$ and $1.01\rho_0$) between the left and right for ideal gas systems approaches to zero for $N_A \gg 1$. In addition, by inserting Eq. (25) into Eq. (26), it follows for the entropy difference ΔS between $S_{[N_A, N_A]}$ and $S_{[0.99N_A, 1.01N_A]}$ that

$$\Delta S \equiv S_{[N_A, N_A]} - S_{[0.99N_A, 1.01N_A]} \approx 0.01N_A k_B \ln \left(\frac{100}{99}\right) > 0. \quad (27)$$

This indicates that the entropy S is the largest for uniform density, and also that S is proportional to the number of molecules.

Now we go back to the comparison of the Helmholtz free energy in Fig. 5. The entropy S is larger for a system with homogeneous density than for an inhomogeneous system, meaning that the right system is advantageous from the entropy aspect. At low temperature, U contribution in Eq. (23) is dominant and the system tries to decrease U to minimize F , whereas at high temperature, the entropy contribution TS overcomes the potential minimization effect. This balance between the potential energy and the entropy governs the basic mechanism of phase separation as well as the surface tension. Note that for ideal gas systems, the potential contribution is constant (zero for the potential in Fig. 3), and the gas molecules tries to fill the system with a homogeneous density to maximize entropy S . Note as well that if a solid surface exists near the droplet at a temperature for the liquid-vapor phase separation, and the droplet is thermodynamically more stable on the surface, a hemispherical droplet is formed on the solid surface, and the equilibrium shape, *i.e.*, the contact angle θ in Fig. 2, is determined so that the total free energy of the system may become minimum depending on the solid-fluid interaction strength.

4 Surface tension

4.1 Bakker's equation

As seen in the above example, we have to inevitably introduce the relation between the free energy of a fluid with interface and the local force to quantitatively evaluate

the surface tension. For that purpose, we set a thought experiment with a flat liquid-vapor interface shown in Fig. 6 for the basic connection between the thermodynamic work as energy and the surface tension. Indeed, such flat interface can easily be achieved by MD simulations by using the periodic boundary condition in the surface lateral directions. In this thought experiment, one piston is set normal to a flat liquid-vapor interface, and it covers from $z = z_L$ to $z = z_V$ at the liquid and vapor bulk regions, respectively, across the plane of the liquid-vapor interface. Another piston parallel to the interface is set in the vapor bulk far from the interface. Through simultaneous virtual infinitesimal displacements of the pistons, only the interface area can be changed without changing the liquid and vapor volumes, V_L and V_V , respectively. Note that the change of bottom area in the figure is not considered. Let l be the depth normal to the xz -plane, and δx be the corresponding displacement of the side piston, the change of interface area A_{LV} writes

$$\delta A_{LV} = l\delta x. \quad (28)$$

In order to let the internal energies before and after the displacement unchanged both for the liquid and vapor parts, this displacement must be done under constant temperature. Then, the net minimum mechanical work δW exerted from the top and side pistons required for this change with quasi-static process can be associated with the change in the Helmholtz energy F . Let γ_{LV} be the LV interfacial energy per area, it follows for the quasi-static change that

$$\delta F = \gamma_{LV}\delta A_{LV}. \quad (29)$$

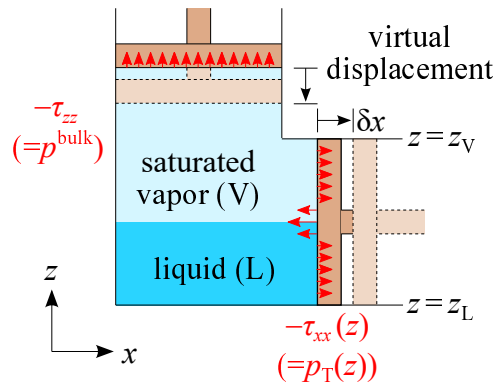
Thus, γ_{LV} writes

$$\gamma_{LV} = \left(\frac{\partial F}{\partial A_{LV}} \right)_{N, V_L, V_V, T}. \quad (30)$$

This means that surface tension is intrinsically a thermodynamic force.

We further relate the mechanical stress changing as a continuous function with the LV interfacial tension γ_{LV} . The fluid stress tensor is not isotropic at phase interfaces

Fig. 6 Thought experiment of Bakker's equation for a flat liquid-vapor interface. The red arrows denote the pressure, *i.e.*, normal fluid stress with its sign inverted, acting on the piston. Reprinted with permission from Yamaguchi *et al.*, J. Chem. Phys. 150, 044701 (2019). Copyright 2019 Author(s), licensed under a Creative Commons Attribution (CC BY) license 4.0 License.



even at equilibrium as shown with the red arrows. Due to the one-dimensional feature of the system along the z -direction, the symmetric stress tensor τ writes

$$\tau = \begin{pmatrix} \tau_{xx} & 0 & 0 \\ 0 & \tau_{yy} & 0 \\ 0 & 0 & \tau_{zz} \end{pmatrix}, \quad (31)$$

where the surface-normal components τ_{zz} is constant in the entire region because of the force balance in the z -direction to be satisfy in the static equilibrium system for the present z -normal flat LV interface system. This constant value is equal to the saturated vapor pressure p^{bulk} with its sign inverted, *i.e.*,

$$\tau_{zz} = -p^{\text{bulk}}. \quad (32)$$

On the other hand, the surface-lateral diagonal components τ_{xx} and τ_{yy} satisfy

$$\tau_{xx}(z) = \tau_{yy}(z) \equiv -p_T(z), \quad (33)$$

where the surface tangential pressure is denoted by $p_T(z)$, which is a unique function of position z and is equal to the isotropic vapor pressure p^{bulk} in the liquid and vapor bulks. We set the liquid and vapor bulk positions at $z = z_L$ and $z = z_V$, respectively. Using these values, the changes of the volume and the Helmholtz free energy as the work upon the quasi-static displacement δx of the side piston are expressed by

$$\delta V = l\delta x \int_{z_L}^{z_V} dz, \quad (34)$$

and

$$dF \equiv \delta W = p^{\text{bulk}}\delta V + l\delta x \int_{z_L}^{z_V} p_T(z) dz, \quad (35)$$

respectively. By inserting Eqs. (28) and (32)-(35) into Eq. (30),

$$\begin{aligned} \gamma_{LV} &= \lim_{\delta x \rightarrow 0} \left. \frac{dF}{dA_{LV}} \right|_{N, V_L, V_V, T} \\ &= p^{\text{bulk}} \int_{z_L}^{z_V} dz - \int_{z_L}^{z_V} p_T(z) dz = \int_{z_L}^{z_V} [p^{\text{bulk}} - p_T(z)] dz \\ &= \int_{z_L}^{z_V} \left[\frac{\tau_{xx}(z) + \tau_{yy}(z)}{2} - \tau_{zz} \right] dz \end{aligned} \quad (36)$$

is derived. Equation (36) is called Bakker's equation, which serves as the basic connection between the microscopic anisotropic stress distribution and the surface tension. Note that the integration range in Eq. (36) is sometimes denoted by $\int_{-\infty}^{\infty}$; however, the necessary condition for this range is that z_L and z_V cover the entire range of the interface with anisotropic fluid stress, *i.e.*, between the liquid and vapor bulks.

4.2 Molecular dynamics simulations

As mentioned in Section 2, molecular dynamics analysis is a powerful choice to overcome the theoretical difficulty of obtaining the equilibrium density distribution in liquid-vapor coexistence systems and resulting stress distribution to calculate the surface tension by Bakker's equation. The left panel of Fig. (7) shows a MD simulation system of Lennard-Jones (LJ) molecules (argon: $\sigma = 0.34$ nm, $\varepsilon = 1.65 \times 10^{-21}$ J in Eq. (11) and $m = 39.948$ g/mol) with flat solid-liquid (SL) and liquid-vapor (LV) interfaces, where 2000 argon molecules were confined in a rectangular simulation cell of $4 \times 4 \times 20$ nm³. The periodic boundary conditions were imposed in the surface lateral x - and y -directions and the mirror boundary condition was set on the top boundary. In addition, a solid wall modelled through an integrated LJ potential was set on the bottom of the system to let the LJ-liquid be adhered on the solid. The system was equilibrated at a temperature of $T = 100$ K ($k_B T / \varepsilon = 0.835$) until the apparent feature of the system did not change. With such setting, one can easily realize a quasi-one-dimensional equilibrium MD system with flat LV and SL interfaces normal to the z -direction.

It is easy to calculate the density of this equilibrium system by taking the time-average of the mass in each flat bin volume set normal to the z -direction with a small thickness of Δz . On the other hand, to calculate the stress, a method called the Method

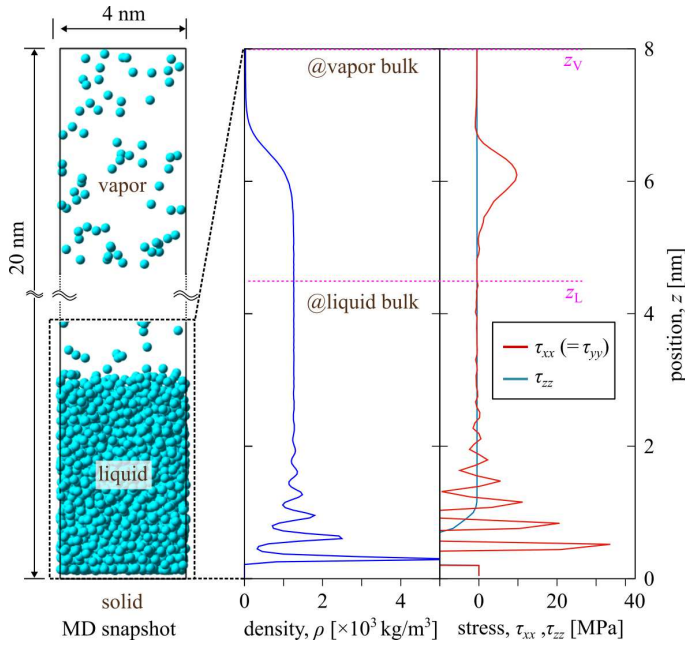


Fig. 7 (Left) snapshot of an equilibrium molecular dynamics simulation system of Lennard-Jones molecules (argon) with flat solid-liquid and liquid-vapor interfaces. (Middle) corresponding density distribution. (Right) distributions of stress diagonal components τ_{xx} and τ_{zz} .

of Plane (MoP) is used, where one sets control surfaces in the system instead of the bin volumes [16, 17]. The local fluid stress tensor $\boldsymbol{\tau}(x, z)$ is calculated by setting z -normal and x - or y -normal flat bin faces in the system in the Cartesian coordinate. Figure 8 shows the schematics of the stress tensor calculation by the MoP. The fluid stress tensor component $\tau_{\alpha\beta}$, which expresses the stress in β -direction exerted on a surface element with an outward normal in α -direction, is given by kinetic term $\tau_{\alpha\beta}^{\text{kin}}$ and inter-molecular interaction term $\tau_{\alpha\beta}^{\text{int}}$ as

$$\tau_{\alpha\beta} = \tau_{\alpha\beta}^{\text{kin}} + \tau_{\alpha\beta}^{\text{int}}. \quad (37)$$

In the MoP, the kinetic term on an α -normal bin face with an area A_α is calculated by

$$\tau_{\alpha\beta}^{\text{kin}} = -\frac{1}{A_\alpha} \left\langle \sum_{i \in \text{fluid}, \delta t}^{\text{across } A_\alpha} \frac{(2\Theta(\mathbf{v}_i \cdot \mathbf{e}_\alpha) - 1) m_i \mathbf{v}_i \cdot \mathbf{e}_\beta}{\delta t} \right\rangle, \quad (38)$$

where m_i and \mathbf{v}_i denotes the mass and velocity vector of i -th fluid molecule, and \mathbf{e}_α and \mathbf{e}_β are the unit normal vectors in α - and β -directions, respectively. The angle brackets means the time average, and the summation $\sum_{i, \delta t}^{\text{across } A_\alpha}$ is taken for every fluid molecule i passing through the bin face within a time interval of δt , which is equal to the time increment for the numerical integration. A switching function $2\Theta(\mathbf{v}_i \cdot \mathbf{e}_\alpha) - 1$, which gives ± 1 depending on the sign of $\mathbf{v}_i \cdot \mathbf{e}_\alpha$ implemented through the Heaviside step function Θ , is included in the RHS of Eq. (38). The meaning of the kinetic stress tensor in Eq. (38) is shown with an example case with $\alpha = x$ and $\beta = y$. Suppose that molecule i with its x -directional velocity v_i^x passes through a x -normal plane from left to right within a time interval δt as in the upper molecule in Fig. 8(a). This is only achieved for positive $v_i^{x(=\alpha)}$ satisfying $\mathbf{v}_i \cdot \mathbf{e}_\alpha > 0$ with

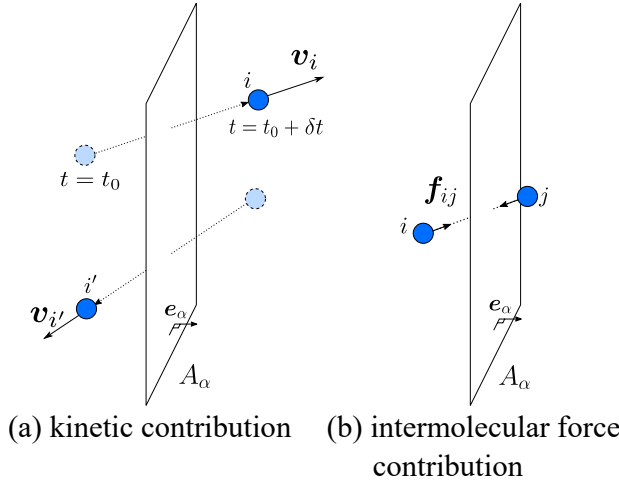


Fig. 8 Schematics of the stress tensor calculation based on the method of plane (MoP).

$\mathbf{e}_\alpha = (1, 0, 0)$, which corresponds to $2\Theta(\mathbf{v}_i \cdot \mathbf{e}_\alpha) - 1 = 1$. Then, the y -directional momentum of the fluid in the left is reduced by $m_i v_i^y$, *i.e.*, is increased by $-m_i \mathbf{v}_i \cdot \mathbf{e}_\beta$ with $\mathbf{e}_\beta = (0, 1, 0)$. This change of momentum is equivalent to the impulse $\tau_{xy} A \delta t$ with the stress tensor. If the passage is in the opposite direction from right to left as in the lower molecule in Fig. 8(a), then, $2\Theta(\mathbf{v}_i \cdot \mathbf{e}_\alpha) - 1 = -1$ and a momentum of $m_i \mathbf{v}_i \cdot \mathbf{e}_\beta$ is given to the fluid in the left. From this formulation, it is known that the kinetic contribution to surface normal stress $\tau_{\alpha\alpha}$ is always negative, *i.e.*, results in positive pressure, and this indeed corresponds to the ideal gas pressure p given in Eq. (5), which is proportional to the density ρ on the face, and is also proportional to the temperature T from Eq. (10).

On the other hand, the intermolecular interaction term in Eq. (37) is given by

$$\tau_{\alpha\beta}^{\text{int}} = -\frac{1}{A_\alpha} \left\langle \sum_{(i,j) \in \text{fluid}}^{\text{across } A_\alpha} (2\Theta(\mathbf{r}_{ij} \cdot \mathbf{e}_\alpha) - 1) \mathbf{f}_{ij} \cdot \mathbf{e}_\beta \right\rangle, \quad (39)$$

where \mathbf{r}_{ij} and \mathbf{f}_{ij} denote the relative position vector $\mathbf{r}_j - \mathbf{r}_i$ and force vector exerted on molecule j at position \mathbf{r}_j from molecule i at \mathbf{r}_i , respectively, and the summation $\sum_{(i,j) \in \text{fluid}}^{\text{across } A_\alpha}$ was taken for all line segments between \mathbf{r}_i and \mathbf{r}_j which crossed the bin face. In contrast to the kinetic contribution, this interaction contribution may give positive surface normal stress $\tau_{\alpha\alpha}$ on the bin face with an attractive interaction \mathbf{f}_{ij} .

The middle and right panels of Fig. 7 shows the density and surface-normal stress distributions, respectively. As expected, the LV interface with a large change in the density has a certain thickness, and in this region with non-constant density, the normal stress τ_{xx} tangential to the interface is different from the bulk stress τ_{zz} , which is constant in the whole system except near the solid at which the fluid is subject to an external force from the solid. Note that a remarkable wiggling structures in the density and stress at bottom is specific to the solid-liquid interface, and this indeed is an interesting topic especially related to the wetting; however, the effect vanishes as leaving away from the solid surface, and we mainly focus on the liquid-vapor interface. It is really amazing that the frontiers could expect the stress distribution at least around the LV interface without MD simulations. Also note that even by such great scientists, quantitatively evaluating the density and stress distributions only from the intermolecular potential was still difficult, and that we have a powerful tool of MD simulations to complement the missing piece. Related to this point, calculating the SL (and SV) interfacial tension from the stress distribution obtained through the MD simulations toward the understanding of wetting is a hot topic at present [18, 19, 20]; however, I will not describe about this in detail considering the scope of this article.

A very simple and intuitive model to explain the stress anisotropy at the liquid-vapor interface, *i.e.*, $\tau_{zz} < \tau_{xx}$, is given here. Suppose z -normal and x -normal planes on a z -normal flat LV interface for the calculation of the normal stress components τ_{zz} and τ_{xx} , respectively based on the MoP as shown in Fig. 9. In this model, we assume average densities ρ_L and $\rho_V (< \rho_L)$ and $\frac{\rho_L + \rho_V}{2}$ in the liquid and vapor bulks and on the interface, respectively for simplicity. In addition, we introduce a

mean-field like approach to the MoP here; instead of counting the molecules passing through the MoP plane for the kinetic stress term τ^{kin} in Eq. (38) or summing up the intermolecular interaction force for the line segment between two molecules crossing the MoP plane for the interaction stress term τ^{int} in Eq. (39), we evaluate τ^{kin} with the density on the point of interest (black cross) on the MoP plane, and τ^{int} with the two densities on the points which sandwich the point of interest (double-headed red arrow) in Fig. 9. As easily imagined, to correctly calculate the latter interaction term of τ^{int} , complicated space integration for the two points using a position- and direction-dependent radial distribution function is needed, and this is indeed the difficulties that the great scientists could not solve analytically, but here we try to represent the interaction term by the most probable single distance in the present simplest model. The kinetic terms τ^{kin} is isotropic in equilibrium systems and is given by

$$\tau^{\text{kin}} = -\frac{Nk_{\text{B}}T}{V}\mathbf{I} = -\rho\frac{k_{\text{B}}T}{m}\mathbf{I}, \quad (40)$$

where \mathbf{I} denotes the identity tensor. Equation (40) corresponds to the ideal-gas pressure, which can be interpreted with Eqs. (10) and (38) as follows: fast molecules giving a momentum of $m\mathbf{v}_i$ in Eq. (38) pass through the plane more with proportional to $|\mathbf{v}_i|$. From Eq. (40), τ_{zz}^{kin} and τ_{xx}^{kin} are identical and those at the LV interface at $z = z_{\text{LV}}$ are expressed by

$$\tau_{zz}^{\text{kin}}(z_{\text{LV}}) = \tau_{xx}^{\text{kin}}(z_{\text{LV}}) = -\frac{\rho_{\text{L}} + \rho_{\text{V}}}{2} \frac{k_{\text{B}}T}{m}. \quad (41)$$

On the other hand, we assume that the interaction term is represented by a single line of interaction force of the most probable distance (double-headed red arrows) which gives an intermolecular force $f_{\text{rep}}(z)$, then the interaction term $\tau_{\alpha\alpha}^{\text{int}}$ writes

$$\tau_{\alpha\alpha}^{\text{int}}(z) \equiv -\rho_1\rho_2c(z)f_{\text{rep}}(z), \quad (42)$$

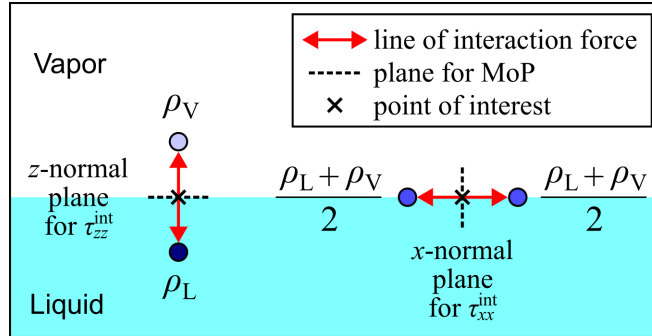


Fig. 9 The simplest model to explain the stress anisotropy at the interface. The interaction terms τ_{zz}^{int} and τ_{xx}^{int} on the point of interest (black crosses) are represented by the interaction between two points having densities $(\rho_{\text{L}}, \rho_{\text{V}})$, and $(\frac{\rho_{\text{L}} + \rho_{\text{V}}}{2}, \frac{\rho_{\text{L}} + \rho_{\text{V}}}{2})$, respectively connected by the double-headed red arrows.

where ρ_1 and ρ_2 are the density of the two points sandwiching the point of interest, and $c(> 0)$ is a certain positive coefficient for the model due to this representation. Note that negative $f_{\text{rep}}(z)$ corresponds to attractive force across the MoP plane to give positive normal stress. Since τ_{zz} must satisfy Eq. (32), $\tau_{zz}(z_{\text{LV}})$ at the interface $z = z_{\text{LV}}$ given by

$$\tau_{zz}(z_{\text{LV}}) = \tau_{zz}^{\text{kin}}(z_{\text{LV}}) + \tau_{zz}^{\text{int}}(z_{\text{LV}}) = -\frac{\rho_{\text{L}} + \rho_{\text{V}}}{2} \frac{k_{\text{B}}T}{m} - \rho_{\text{V}}\rho_{\text{L}}c(z_{\text{LV}})f_{\text{rep}}(z_{\text{LV}}) \quad (43)$$

with $(\rho_1, \rho_2) = (\rho_{\text{L}}, \rho_{\text{V}})$ in Eq. (42), is equal to $\tau_{zz}(z_{\text{V}})$ in the vapor bulk at $z = z_{\text{V}}$, corresponding to the saturated vapor pressure. This is given by

$$\tau_{zz}(z_{\text{V}}) = \tau_{zz}^{\text{kin}}(z_{\text{V}}) + \tau_{zz}^{\text{int}}(z_{\text{V}}) = -\rho_{\text{V}} \frac{k_{\text{B}}T}{m} - \rho_{\text{V}}^2 c(z_{\text{V}})f_{\text{rep}}(z_{\text{V}}) \approx -\rho_{\text{V}} \frac{k_{\text{B}}T}{m}, \quad (44)$$

where the interaction term is assumed to be zero for the last approximation considering that the intermolecular interaction in the vapor is negligible. Thus, it follows

$$c(z_{\text{LV}})f_{\text{rep}}(z_{\text{LV}}) = -\frac{\rho_{\text{L}} - \rho_{\text{V}}}{2} \frac{k_{\text{B}}T}{m} < 0, \quad (45)$$

indicating that $f_{\text{rep}}(z_{\text{LV}})$ is negative, *i.e.*, the representative interaction across the MoP plane at the LV interface is attractive. Assuming as well that $c(z_{\text{LV}})f_{\text{rep}}(z_{\text{LV}})$ is independent of the direction at z_{LV} , then the normal stress lateral to the interface writes

$$\tau_{xx}|_{z=z_{\text{LV}}} = -\frac{\rho_{\text{L}} + \rho_{\text{V}}}{2} \frac{k_{\text{B}}T}{m} - \left(\frac{\rho_{\text{V}} + \rho_{\text{L}}}{2}\right)^2 c(z_{\text{LV}})f_{\text{rep}}(z_{\text{LV}}). \quad (46)$$

Using the relation between the arithmetic and geometric means

$$\rho_{\text{L}}\rho_{\text{V}} < \left(\frac{\rho_{\text{L}} + \rho_{\text{V}}}{2}\right)^2, \quad (47)$$

it follows for $\tau_{zz}(z_{\text{LV}})$ and $\tau_{xx}(z_{\text{LV}})$ in Eqs. (43) and (46), respectively that

$$\tau_{zz}(z_{\text{LV}}) < \tau_{xx}(z_{\text{LV}}). \quad (48)$$

This inequality is a simple model to explain the stress anisotropy shown in Fig. 7, due to the density anisotropy, and this is the fundamental basis of Bakker's equation (36).

The left panel of Fig. (10) shows the distributions of the normal stress τ_{xx} tangential to the interface and density ρ at three different temperature $T = 90, 95$ and 100 K enlarged around the LV interface. As the temperature increases, the stress difference between the values of $\tau_{xx}(z)$ at the interface and away from the interface becomes smaller. The latter away from the interface is equal to and τ_{zz} , which is equal to the constant stress value away from the LV interface as shown in Fig. 7. From Bakker's equation (36), this means that the LV interfacial tension γ_{LV} decreases with the temperature rise. Note also that the bulk liquid density decreases with the temperature rise, and this is related to the increase of the average distance upon temperature rise indicated in Fig. 4. In addition, the bulk stress decreases with the

temperature rise, and this means that the saturated vapor pressure p_V^{bulk} given by Eq. (32) increases with temperature. Such basic features are indeed realized in the MD systems.

The right panel of Fig. 10 shows the LV interfacial tension γ_{LV} and p^{bulk} at different temperature T . As expected from the right panel, γ_{LV} decreases and p^{bulk} increases with the temperature increase. The vapor pressure is above the atmospheric pressure, and the extraordinary high anisotropic local stress τ_{xx} gives the interfacial tension around 10 mN/m, and the resulting temperature dependence of about -0.2 mN/m·K. Of course, the absolute value and the coefficient of the temperature dependence depend on the molecular type and temperature range, but in general, this non-negligible temperature gradient gives the local stress gradient around the interface known as the temperature Marangoni effect, which drives the liquid flow from a higher-temperature region to a lower-temperature region.

5 Concluding remarks

Surface is physically as well as theoretically at the boundary of macroscopic and microscopic physics, understanding of surface tension intrinsically needs multiple knowledge of thermodynamics, statistical mechanics as well as continuum mechanics. In this article, after introducing the interpretation of the phase change, liquid-vapor coexistence and interfacial tension from these points of view, molecular dynamics results were shown which indicate the existence of microscopic stress anisotropy at the interface as the origin of the macroscopic stress surface tension tan-

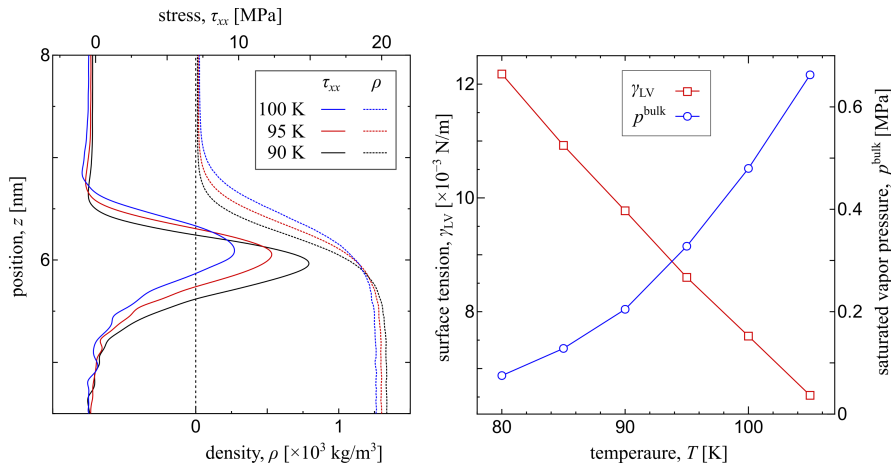


Fig. 10 (Left) distributions of the normal stress τ_{xx} tangential to the interface and density ρ at three different temperature $T = 90, 95$ and 100 K enlarged around the LV interface. (Right) liquid-vapor interfacial tension γ_{LV} and p^{bulk} at different temperature T .

gential to the interface. In addition, a simple model to explain the stress anisotropy due to the density anisotropy was provided. At present, molecular dynamics as a powerful tool is available, and I hope that unsolved issues about this fascinating physics, especially related to the Marangoni effect and wetting, will be elucidated.

Acknowledgements The simulation results in this article are provided by Minori Shintaku and Yule Ding, former members of the author's group. I sincerely appreciate their cooperation.

References

1. Marchand, A., Weijss, J. H., Snoeijer, J. H., Andreotti, B.: Why is surface tension a force parallel to the interface?. *Am. J. Phys.* **79**, 999–1008 (2011)
2. de Gennes P.-G., Brochard-Wyart, F., Quere, D.: *Capillarity and Wetting Phenomena: Drops, Bubbles, Pearls, Waves* Springer, Berlin (2003)
3. Gao, L., McCarthy, T. J.: Wetting 101°. *Langmuir* **25**, 14105–14115 (2009)
4. Thompson, A. P., Aktulga, H. M., Berger, R., Bolintineanu, D. S., Brown, W. M., Crozier, P. S., in't Veld, P. J., Kohlmeyer, A., Moore, S. G., Nguyen, T. D., Shan, R., Stevens, M. J., Tranchida, J., Trott, C., Plimpton, S. J.: LAMMPS - a flexible simulation tool for particle-based materials modeling at the atomic, meso, and continuum scales. *Comp. Phys. Comm.* **271**, 108171 (2022).
5. <http://www.gromacs.org>
6. Rowlinson, J. S.: "Cohesion: A Scientific History of Intermolecular Forces. Cambridge University Press (2002)
7. Ono, S.: *Surface tension*. Kyoritsu, Tokyo (1980) (in Japanese).
8. Young, T.: III. An essay on the cohesion of fluids. *Philosophical Transactions of the Royal Society of London* **95**, 65–87 (1805)
9. Bernoulli, D.: *Hydrodynamica, sive de viribus et motibus fluidorum commentarii : Opus Academicum*.
10. Fujiwara, K., Hyodo, T.: *Introduction to Thermal Physics, From a Macroscopic to Microscopic Approach*. University of Tokyo Press, Tokyo (1995) (in Japanese).
11. van der Waals, J. D.: *Thermodynamische theorie der capillariteit in de onderstelling van continue dichtheidsverandering*. Verhandel. Konink. Akad. Wet. Amsterdam (Sect. 1), Vol. 1, No. 8 (1893)
12. Rowlinson, J. S.: Translation of J. D. van der Waals' "The Thermodynamic Theory of Capillarity Under the Hypothesis of a Continuous Variation of Density." *J. Stat. Phys.* **20**, 197–200 (1979)
13. Ono, S., Kondo, S.: *Molecular Theory of Surface Tension in Liquids*. pp. 134–280. Springer, Berlin (1960)
14. Rowlinson, J. S., Widom, B.: *Molecular Theory of Capillarity*. Dover, New York (1982)
15. Wilhelmy, L.: Über die Abhängigkeit der Capillaritäts-Constanten des Alkohols von Substanz und Gestalt des benetzten festen Körpers, *Ann. Phys.* **195**, 177–217 (1863)
16. Thompson, S. M., Gubbins, K. E., Walton, J. P. R. B., Chantry, R. A. R., Rowlinson, J. S.: A molecular dynamics study of liquid drops, *J. Chem. Phys.* **81**, 530–542 (1984)
17. Yaguchi, H., Yano, T., Fujikawa, S.: Molecular Dynamics Study of Vapor-Liquid Equilibrium State of an Argon Nanodroplet and Its Vapor, *J. Fluid. Sci. Tech.* **5** 180–191 (2010)
18. Surblys, D., Yamaguchi, Y., Kuroda, K., Kagawa, M., Nakajima, T., Fujimura, H.: Molecular dynamics analysis on wetting and interfacial properties of water-alcohol mixture droplets on a solid surface, *J. Chem. Phys.* **140**, 034505 (2014)
19. Yamaguchi, Y., Kusudo, H., Surblys, D., Omori, T., Kikugawa, G.: Interpretation of Young's equation for a liquid droplet on a flat and smooth solid surface: Mechanical and thermodynamic routes with a simple Lennard-Jones liquid, *J. Chem. Phys.* **150**, 044701 (2019)

20. Kusudo, H., Omori, T., Yamaguchi, Y.: Local stress tensor calculation by the method-of-plane in microscopic systems with macroscopic flow: A formulation based on the velocity distribution function, *J. Chem. Phys.* **155**, 184103 (2021)